Published in final edited form as:
Anal Chem. 2008 April 15; 80(8): 2717–2727. doi:10.1021/ac7021184.

Glucose and Lactate Biosensors for Scanning Electrochemical Microscopy Imaging of Single Live Cells

Madalina Ciobanu[1], **Dale E. Taylor Jr.**[2], **Jeremy P. Wilburn**[1], and **David E. Cliffel**[1,*]

[1] Department of Chemistry, Vanderbilt University, Nashville, TN 37235

[2] Department of Chemistry and Life Science, United States Military Academy, West Point, NY 10996

Abstract

We have developed glucose and lactate ultramicroelectrode (UME) biosensors based on glucose oxidase and lactate oxidase (with enzymes immobilized onto Pt UMEs by either electropolymerization or casting) for scanning electrochemical microscopy (SECM), and have determined their sensitivity to glucose and lactate, respectively. The results of our evaluations reveal different advantages for sensors constructed by each method: improved sensitivity and shorter manufacturing time for hand-casting, and increased reproducibility for electropolymerization. We have acquired amperometric approach curves (ACs) for each type of manufactured biosensor UME, and these ACs can be used as a means of positioning the UME above a substrate at a known distance. We have used the glucose biosensor UMEs to record profiles of glucose uptake above individual fibroblasts. Likewise, we have employed the lactate biosensor UMEs for recording the lactate production above single cancer cells with the SECM. We also show that oxygen respiration profiles for single cancer cells do not mimic cell topography, but are rather more convoluted, with a higher respiration activity observed at the points where the cell touches the Petri dish. These UME biosensors, along with the application of others already described in the literature, could prove to be powerful tools for mapping metabolic analytes, such as glucose, lactate and oxygen, in single cancer cells.

Keywords

scanning electrochemical microscopy; ultramicroelectrode; biosensor; enzyme; glucose sensor; lactate sensor; cellular respiration

INTRODUCTION

The past decade has witnessed a growth in the application of biosensors to micron and submicron level investigations in a wide variety of disciplines. Rapid development, both in miniaturization techniques and in understanding of biological processes, has accelerated the expansion of biosensors in clinical applications and in areas such as biology, neurobiology, pharmacology, and tissue engineering.[1,2] In this respect, researchers have been able to acquire real-time quantitative measurements through the application of micro-sensors on living cells, both in vitro and in vivo.[2–4]

Of particular interest are the enzyme-based sensors because they offer the selectivity toward a single analyte optimized by natural evolution. Enzymes achieve molecular recognition of substrates (i.e., analytes of interest) based on structural complementarity, leaving little room

d.cliffel@vanderbilt.edu.

for error.[5] Enzymes catalyze with high specificity chemical reactions in biological systems according to Equation 1:

$$\text{substrate} + \text{cofactor} \xrightarrow{enzyme} \text{products} \quad (1)$$

Enzymes have been successfully employed in the miniaturization of sensor designs, including one of the most important sensors for the health industry that emerged decades ago: the glucose sensor which is based on glucose oxidase (GOx), whether it is intended for in vivo monitoring of glucose levels,[6] or for a diabetic's regular glucose meter for use at home. Besides GOx, there have been numerous other enzymes used for the development of miniaturized amperometric sensors, such as sarcosine oxidase,[7] galactose oxidase,[7] hexokinase,[8] choline oxidase,[7] lactate oxidase (LOx),[9] alcohol oxidase,[7] horseradish peroxidase,[10] cholesterol oxidase,[11,12] etc.

In addition to their importance for diabetes patients and in vivo studies, enzyme-based amperometric sensors are irreplaceable tools for the non-invasive study of the metabolism at the cellular level. A simplified view of the metabolic processes at the single cell level is presented in Figure 1, indicating that information about the way a cell performs glycolysis could be acquired by using enzyme-based sensors for glucose and lactate. We have already employed GOx and LOx based sensors for probing cellular metabolism in a multianalyte microphysiometer (MAMP).[13–16] Our laboratory has modified the Cytosensor™ microphysiometer (originally developed by Molecular Devices for the measurement of acidification rates) into the MAMP to allow for simultaneously recording four analytes: glucose and oxygen uptake, lactate production and extracellular acidification rates for large numbers ($> 10^5$) of cells. The MAMP proves a useful tool in studies such as the response of various cell types to chemical agents and toxins with ramifications in biodefense studies;[15] cancer cellular metabolism relating genetic mutations to different metabolic phenotypes, with implications in mathematical modeling of cancer.[17,18] The MAMP yields metabolic rates (e.g., lactate production rate) for large number of cells, but has no ability to assess cell to cell variability. This paper is not a study of the variability of metabolic rates from one single cell to another, but rather it presents the technical means that could be employed for addressing this problem by opening up the range of analytes for single cell electrochemistry.

The glucose and lactate amperometric sensors are based on a Pt electrode that is in contact with a polymer containing the specific enzyme (Figure 2); glucose and lactate are measured indirectly at the electrode surface by amperometric oxidation of hydrogen peroxide. The hydrogen peroxide is formed in aqueous environments during the reaction catalyzed by the enzyme entrapped in the matrix (e.g., GOx in Figure 2A or LOx in Figure 2B) with the analyte of interest (i.e., glucose for Figure 2A or lactate for Figure 2B) in aerobic conditions, as described by Equations 2 and 3:

$$\text{D} - \text{glucose} + \text{oxygen} \xrightarrow{GOx} \text{D} - \text{gluconolactone} + \text{hydrogen peroxide} \quad (2)$$

$$\text{L} - \text{lactate} + \text{oxygen} \xrightarrow{LOx} \text{pyruvate} + \text{hydrogen peroxide} \quad (3)$$

Horrocks et al.[10] have used an enzyme (horseradish peroxidase) UME in conjunction with the scanning electrochemical microscopy (SECM) for the measurement of H_2O_2 at surfaces. They do not present any amperometric approach curves (ACs), but rather conductance-distance curves. The conductance measurements have the advantage of being insensitive to the enzyme-

polymer layer present on the tip, however, they have to be performed in solutions of very low conductivity (1 mM KCl) which makes them unsuitable for physiological applications, such as approaching and imaging in biological buffers (e.g., RPMI). Kueng et al.[8] have also reported the use of an enzyme UME for SECM; they have assembled a Pt dual microdisk electrode with one 5 μm Pt for electrode positioning via ACs and with the other 5 μm Pt modified through electropolymerization with both GOx and hexokinase for indirect imaging of ATP transport through a porous polycarbonate membrane. However, they have not used the enzyme sensor of this dual UME for either approaching the surface nor for imaging of live organisms. Acquiring ACs using the electrochemical process that takes place at an enzyme modified tip would remove the need in this case for manufacturing the more complicated dual UME. Kueng et al.[19] have also used an enzyme (GOx) coated tip integrated in an AFM-SECM setup for imaging glucose transport through a porous membrane; in this case they bypassed the need for ACs by using the AFM tip.

SECM[20–23] can be developed as a useful technique for the study of cell metabolic fluxes (as an important component of metabolomics), since it can map electrochemical activity across the entire surface of a single cell, and can record dynamic changes. Although SECM has been used over the years for investigating biological systems,[23,24] only recently has attention been given to SECM for single cell studies.[25–38] Mirkin et al.[26,27,32–34] have investigated single cells by SECM in order to determine various redox activities across different types of cells, examining the differences between nonmetastatic and metastatic human breast cells. They have identified series of redox mediators that can cross the cell membrane, investigated their distribution between cytosol and nucleus, and found them unable to penetrate the nuclear envelope. Matsue et al.[36–38] studied single cell topography and paid particular attention to respiration studies by means of SECM for cells such as protoplasts and PC12. Wipf et al.[31] have used SECM to monitor the real-time morphological changes in PC12 cells that are used as model neurons. Baur et al.[30] have used a constant distance SECM for a study of PC12 cells where they showed that constant impedance imaging yields superior topographic images of single cells compared to more common constant height SECM. Schuhmann et al.[28] recorded topographic images of PC12 cells by SECM, and studied catecholamine release from PC12 cells, using SECM as a positioning tool for an amperometric sensor in the vicinity of the cells. Isik and Schuhmann[29] have detected the release of nitric oxide from single T-HUVEC cells by also using a constant distance SECM. Bard et al. have used SECM to study the metabolism of menadione to thiodione in single hepatoblastomas,[35] and have probed the activity of HeLa cells using the oxidation of a ferrocene derivative.[25]

Our choice of using the constant height SECM versus the constant distance SECM for the study of single cell metabolism was predicated on using a chemically modified tip (i.e., Pt UME coated with an enzyme-containing polymer); the modified tips can be integrated easier with the typical constant height SECM mode of operation. The major ways of achieving the constant distance mode in SECM are all relatively limited for the distance signal possibilities, due to their intrinsic design. One possibility for the constant distance mode is the use of the impedance SECM,[39] which is based on acquiring data based on high frequency capacitance measurements. The capacitance of the chemically modified tips would be dramatically affected by the presence of the polymer layer entrapping the enzymes on the Pt UME, compared to bare metal tips. Another way of achieving the constant distance mode for SECM measurements is by using shear force.[40] Hengstenberg et al. have shown that enzyme-filled capillaries can be used as tips for scanning using a shear force based constant distance SECM mode;[41] however, these tips are not amperometric and are suited to generation-collection modes, not imaging. The application of a polymer film to the tip for shear force based SECM applications appears technically challenging because the mass loading of the enzyme film will reduce the resonant Q of the oscillating tip in addition to the hydrodynamic loss in Q from a large volume of solution above the cells. Another mode of operation for the SECM would be the AFM-SECM.[42] While

Kueng et al. reported a GOx-coated AFM tip,[19] the use of AFM-SECM for scanning live cells has yet to be developed into a practicable method, and the difficulty of making each tip by FIB micromachining is considerable. The integration of polymer film-modified tips for use in conjunction with a constant distance SECM for the study of live cell metabolism will be the subject of future studies. With the typical UME sizes of 5–25 μm used in our work, the higher resolution possible by constant distance control would not be significant, justifying our use of constant height imaging.

A single cell is the basic structural and functional unit of all organisms. While the MAMP provides information about the metabolism of cells, it averages signals over large populations (> 10^5 cells) and cannot distinguish differences between individual cells. One cannot develop a deep understanding of metabolomics unless the processes are explored in the context of the individual cell level, wherein multiple biochemical processes, distributed throughout the cell and various cell compartments, are integrated into a functional system. Differences in the average rate of glycolysis between large numbers of cancerous and healthy cells have been demonstrated,[43,44] making spatio-temporal mapping of glycolytic analytes (e.g., pH, lactate, oxygen, glucose) an area of great interest. The intracellular pH for both cancerous and normal cells is approximately 7.4,[45] and the extracellular pH for cancerous growths is acidic, with values as low as 6.7.[46] This increased acidity in tumors is a result of the Warburg effect,[44] i.e., enhanced glycolysis, which under hypoxic conditions leads to an increased lactate production that in turn lowers the extracellular pH (Figure 1). Walenta et al.[47] reported mean lactate concentrations in head and neck tumours of ~ 12 μmol/g, as compared to similar normal tissue lactate concentrations of ~ 5 μmol/g. Acidity profiles[32] were previously studied by SECM for single living cells; however, the recording of these pH profiles presents certain technical difficulties, such as the use of an additional potentiostat in conjunction with the SECM, as the pH sensor (Sb-based in Liu et al.'s paper)[32] is by definition potentiometric. Using the lactate production to characterize cancer cells presents its own advantages, such as the use of an amperometric sensor for lactate sensing, the ability to record lactate profiles in highly buffered solutions (as most cell culture media are) as opposed to a pH potentiometric sensor that can be used solely in a modified low buffered medium. Lactate production profiles could also provide information that could lead to a deconvolution of the pH profiles of cancerous cells.

Cell respiration[37] was also previously studied by SECM for single living cells; however, to our knowledge, there have been no reported glucose or lactate spatio-temporal profiles for single live cells. We present in this paper the manufacturing and characterization of glucose and lactate ultramicroelectrode biosensors for SECM of single live cells, and demonstrate that the GOx-based sensors can be used for the positioning of the UME in the vicinity of the cell, as well as for the imaging of the cell, and also show that the LOx-based sensors can be used for recording of lactate release profiles from single cells.

EXPERIMENTAL SECTION

Materials

The materials were purchased as follows: $MgCl_2 \cdot 6H_2O$, $NaH_2PO_4 \cdot H_2O$, HCl, $CaCl_2$, $MgSO_4$, NaCl, KCl, KH_2PO_4, $NaHCO_3$, L-lactic acid, sodium acetate trihydrate, 35 mm Petri dishes and 50 mM phosphate buffer pH 7.0 from Fisher Scientific; KPF_6 from Aldrich Chemical; glutaric dialdehyde as 25% solution in water (GDA) and 2-aminophenol (OAP) from Acros; $Na_2HPO_4 \cdot 7H_2O$, bovine serum albumin (BSA), RPMI 1640, D-glucose, GOx, type II-S from *Aspergillus niger* and LOx from *Pediococcus* species from Sigma; H_2SO_4 and NaOH from EM Science; ethanol (absolute proof) from Aaper; ferrocenylmethyltrimethylammonium iodide from Strem Chemicals; N_2 from Gibbs Welding Supply; conductive silver epoxy from Epoxy Technology; white sealant Hysol Epoxi-Patch

from Dexter Corporation; 35 mm glass bottom Petri dishes from Bioscience Tools. All materials were used as received unless otherwise specified.

ASTM Type I (18 MΩ) analytical grade deionized water (DW) was obtained with a Solution 2000 Water Purification System from Solution Consultants. All solutions were filtered prior to use with 0.2 μm syringe filters from Fisher. Ferrocenylmethyltrimethylammonium hexafluorophosphate (FcTMA) was prepared according to the method of Mirkin and co-workers.[48]

All reported potentials were measured against a commercial Ag/AgCl, 3 M KCl reference electrode (RE, model CHI111, CH Instruments).

SECM testing prior to converting UMEs into biosensors

All SECM measurements were conducted with a CHI900 instrument from CH Instruments equipped with an adjustable stage for tilt correction. The electrochemical cell was in a typical four-electrode configuration for testing the UMEs: UME tip electrode (working electrode, WE), Pt wire counter electrode (CTR), Ag/AgCl, 3 M KCl (RE), and substrate electrode (SE), which was a 2 mm Pt disk (CHI303). All UMEs were manufactured with 5 or 25 μm Pt wire from Goodfellow according to Bard et al.,[21] polished with 0.05 μm alumina from Buehler, and sonicated in ethanol and water. UMEs were electrochemically cleaned for 5 min in 0.5 M H_2SO_4 using a CHI660a potentiostat, and were tested with 1 mM FcTMA in 100 mM KCl for performance. The Pt SE was polished and cleaned in an identical manner to the UMEs. Only UMEs capable of achieving $I_T = 8$ (e.g., 800% increase in current over steady-state conditions far from the SE)[23] during approach to the Pt SE were used in biosensor construction. The UMEs were also characterized by cyclic voltammetry (CV), and consistently yielded the expected sigmoidal CV. The UMEs used had RG ratios[21] of ≃ 5 for the 5 μm Pt tips (7 μm actual measured diameter) and ≃ 2 for the 25μm Pt tips.

Enzyme-based UMEs. (a) Manufacturing

The enzyme-containing polymer layer was deposited onto 25 μm Pt UMEs via two distinct methods: (i) Electropolymerization – the enzyme was deposited on the electrode in a similar manner as described by Zhang et al.[49] The enzyme (10 mg/mL for GOx and 2 mg/mL for LOx) and the OAP (0.8 mg/mL) were dissolved in 50 mM acetate buffer, pH 5.9, the solution was degassed (N_2), and the electrodeposition occurred under stirring at E = +0.65 V vs. Ag/AgCl, 3 M KCl for 1 hour (CHI660a workstation equipped with a Faraday cage); the electrodes were allowed to dry for another hour, were then briefly rinsed with DW and stored at 4 °C in 50 mM phosphate buffer until use. (ii) Casting – the enzyme (8 mg/mL for GOx and 10 mg/mL for LOx), GDA (14 μL/mL buffer) and BSA (62.5 mg/mL) were all dissolved in 50 mM phosphate buffer, pH 7.0;[16] the enzyme solution was then hand-cast onto the surface of the UME by briefly touching the tip of the UME to a tiny droplet of enzyme solution; the UMEs were air dried and stored at room temperature until further use. **(b) Calibrations.** The performance of the biosensor UMEs was tested using a CHI660a potentiostat with a three electrode configuration: WE – enzyme UME; RE - Ag/AgCl, 3 M KCl; CTR – Pt mesh. Current vs. time curves were recorded under moderate stirring at E = + 0.6 V vs. Ag/AgCl, 3 M KCl (for both GOx and LOx). Standard additions were made from stock solutions of 500 mM glucose and 100 mM lactate. To ensure the validity of the results, the calibrations were performed before and after the use of the biosensor UMEs in conjunction with the SECM.

SECM approach curves of biosensor UMEs

ACs were acquired for GOx and LOx UMEs in a three-electrode system: WE – biosensor 25 μm UME; RE - Ag/AgCl, 3 M KCl; CTR – Pt mesh. The tip was approached to the substrate

(35 mm Petri dish) and allowed to touch it. Glucose solutions of 1.0–5.0 mM and lactate solutions of 0.5 mM were used in the approach experiments.

Cells

Fibroblasts (mouse fibroblast CRL-10225) were cultured in high glucose (4.5 g/L) DMEM (Dulbeco's modified Eagle's medium) with 4 mM L-glutamine, supplemented with 10 % fetal bovine serum and 1.0 mM sodium pyruvate. MCF10CA1a cells[50] were cultured in DMEM/F12 medium, supplemented with cholera toxin (0.1 μg/mL), insulin (10 μg/mL), hydrocortisone (0.5 μg/mL), epidermal growth factor (20 ng/mL) and horse serum (5 %). PC12 cells (CRL-1721) were cultured in Ham's F12K medium with 2 mM L-glutamine adjusted to contain 1.5 g/L sodium bicarbonate (82.5 %), horse serum (15 %), and fetal bovine serum (2.5 %); PC12 cells were plated on dishes treated with human collagen (type IV).

SECM imaging

The SECM was used in conjunction with an inverted microscope (VistaVision, VWR) equipped with a stage and objective warmer (TCII, 2Ch micro temperature controller, Bioscience Tools). The inverted microscope allowed for visually monitoring the morphology of the cells to be scanned. The SECM tip holder was extended above the microscope objective with the aid of a light but sturdy aluminum piece. For positioning, the UMEs were approached to the dish and then withdrawn a known distance. The data were recorded in a three-electrode system: WE – UME; RE - Ag/AgCl, 3 M KCl; CTR – Pt mesh, in the constant height mode. **(a) Glucose profiles.** The 25 μm UME GOx biosensors were positioned near the cell to be imaged, and then the biosensor tip was rastered across the surface above the cell while the tip was maintained at E = + 0.6 V vs. Ag/AgCl, 3 M KCl. The buffer used was Hank's balanced salt solution (HBSS), pH 7.4, 5 mM glucose and no phenol red. **(b) Lactate profiles.** The 25 μm UME LOx biosensors were positioned near the cell to be imaged, and then the biosensor tip was rastered across the surface above the cell while the tip was maintained at E = + 0.6 V vs. Ag/AgCl, 3 M KCl. The buffer used was RPMI, pH 7.4; there was no lactate added/present in the solution. There are possible interfering analytes secreted by the cells (e.g., peroxide, dopamine, etc.) that would be active at the potential set for the UME biosensor. However, the types of sensors we are using are enzyme-based, and the polymer films are highly selective, as the polymer helps to block interferents. We have extensively tested the use of the sensors in the presence of live cells in the MAMP and found no analyte detection problems due to cross-interferents at this potential.[14–16] **(c) Oxygen profiles.** The buffer used was HBSS, pH 7.4, with 5 mM glucose and 1 mM FcTMA. The Pt 7 μm UME was used for recording topographical images first, with the tip potential E = + 0.6 V vs. Ag/AgCl, 3 M KCl, ensuring the oxidation of the FcTMA. We chose FcTMA as mediator for topography imaging of single cells based on previous work in our lab showing that this particular redox mediator does not cross bilayer lipid membranes (BLMs),[51] i.e., it yields a negative feedback when the UME approaches the BLM. Once the SECM topography information was acquired, the tip potential was switched to E = − 0.5 V vs. Ag/AgCl, 3 M KCl, ensuring the reduction of the oxygen present in the solution, thus yielding oxygen uptake profiles.

RESULTS AND DISCUSSION

We have manufactured GOx enzyme UME biosensors by employing two methods: electropolymerization and hand casting. We have tested the properties of the enzyme films deposited onto the Pt UMEs by doing amperometric calibrations prior to any SECM applications. Figure 3A displays a typical example of a calibration toward the analyte of interest (i.e., glucose) of an electropolymerized GOx UME biosensor. The sensor displays linear sensitivity to glucose for concentrations of up to 18 mM, and there is no response to blank additions (buffer, no glucose). In order to find the "zero distance point" on the AC, the sensors

were allowed to approach until they physically touched the substrate surface. In order to determine whether the procedure adversely affected performance, after the SECM experiments the sensors were tested again for sensitivity with respect to their analyte. Figure 3B shows an example of amperometric calibration for a GOx UME sensor after use in conjunction with SECM for recording ACs. The sensor UME continues to display linear sensitivity to glucose for concentrations of up to 18 mM, and there is no response to the blank additions. Comparatively, the cast GOx UME biosensors display a narrower linear sensitivity range, for glucose concentration of up to 14 mM. Figure 3C presents the stability of an electropolymerized GOx UME sensor in time. The data points in Figure 3C have been obtained from amperometric calibration curves similar to the ones presented in Figures 3A and 3B. Figure 3C displays one measurement (data point) for each day for each concentration represented on the graph. The electrode was stored in the refrigerator in 50 mM phosphate buffer pH 7 between runs. There is little difference between the calibrations done over the course of 12 days, and this minute variation is not important in the context of the fact that the electrodes should always be calibrated the day of the measurements. The electropolymerized GOx sensors (if stored at 4 °C in buffer) preserve their sensitivity toward glucose for periods of time for up to 1 month. In contrast, the cast 25 μm GOx sensors (stored at room temperature, no buffer) start to lose sensitivity to glucose after 2–3 days. Different storage conditions have been explored for all types of sensors presented in this paper, and the optimum ones for each sensor type are the only ones discussed here (dry storage at room temperature for hand-cast biosensors, and 4 °C in buffer for electropolymerized biosensors). One advantage that the cast GOx sensors have over the similar electropolymerized ones is the more facile manufacturing procedure, which renders the films applied on the 25 μm Pt UME as ‘disposable.’ The overall success rate for production of sensors (determined by whether sensors exhibited sensitivity toward their analyte the same day as manufacturing) was ~ 70 % for the electropolymerization process and ~ 90 % for the casting method (we have tested at least 20 electrodes for each method).

The lactate sensor production is complicated by the relatively lower stability of LOx as compared to GOx. Figure 4 compares the behavior of electropolymerized and cast LOx UME sensors. For both types of LOx-based sensors, the calibration plots seem to exhibit two distinct linear ranges: 0.1 – 0.3 mM that covers the likely physiological range for single cell release, and 0.4 – 0.9/1.0 mM lactate, which may be useful for future studies (e.g., scanning across surfaces with patterned LOx, in the presence of lactate in solution). Horrocks and co-workers[10] have observed the same type of dual range when they calibrated a horseradish peroxidase-modified UME with respect to H_2O_2 sensitivity; they have proposed that this decay in sensitivity was due to the redox process in parts of the polymer in poor contact with the UME element (carbon fiber in their case). The electropolymerized LOx sensors generally lose sensitivity to lactate above 0.9 mM lactate (Figure 4A). However, these UME sensors are assembled with the help of oxidases, and as such they should obey the enzyme kinetics laws. For enzymes following the Michaelis-Menten behavior, one should look at the Lineweaver-Burk double reciprocal plot, where the inverse of the reaction rate is directly proportional to the inverse of the substrate concentration[5] (e.g., lactate in our case). Since the reaction rate is directly proportional to the current,[52] we can plot the inverse of the current versus the inverse of the lactate concentration, for example, and if the plot is linear, then the enzyme follows the Michaelis-Menten kinetics. Figure 4C displays the data from Figure 4A in the form of the Lineweaver-Burk double reciprocal plot, and Figure 4D does the same thing for the data from Figure 4B (before SECM). Both plots appear linear, indicating that the presence of two distinct regions in Figures 4A and 4B are due to a saturation of the LOx enzyme with the lactate substrate, meaning that the enzymes follow the Michaelis-Menten kinetics. The R^2 values for the Lineweaver-Burk double reciprocal plots in both cases (Figures 4C and 4D) are higher than the R^2 values for the linear ranges corresponding to the higher concentrations (> 0.4 mM, Figures 4A and 4B), indicating that these films should be regarded as obeying the Michaelis-Menten behavior, rather than having two distinct linear regions as it was previously suggested.

[10] Since the concentration of lactate production by cells is very low, the concentrations of produced lactate are contained in the lower regions (below 0.3 mM lactate), which are linear under the Michaelis-Menten behavior, and thus the enzyme saturation with the substrate does not hinder the detection for our purposes.

Just as for the GOx UME biosensors, we have tested the properties of the LOx sensors before and after the use in conjunction with the SECM, to validate the SECM results. Figure 4B displays examples of calibration plots for a cast LOx UME biosensor in the lower linear concentration range before and after recording ACs (where the tip was allowed to touch the Petri dish substrate in order to find the "zero distance point"), showing that sensitivity toward lactate is retained. While the electropolymerized LOx sensors are more reproducible, they have a lower life time (~ 24 h, stored at 4 °C in buffer) compared with the cast LOx sensors (2 days, room temperature). The manufacturing success rate is overall lower for the LOx sensors than for the GOx sensors: ~ 20 % for electropolymerized LOx and ~ 60 % for cast LOx sensors (we have tested at least 20 electrodes for each method). Just as in the case of the GOx sensors, the cast LOx sensors are easier to manufacture than the electropolymerized ones, and the cast LOx films can be regarded as 'disposable.'

As expected, for both types of sensors discussed in this paper, the electropolymerized ones were more reproducible than the cast ones. During the casting procedure it is difficult to control the exact amount of enzyme solution that gets deposited onto the Pt tip and/or the casting solution homogeneity (for electrodeposition the solution is stirred). However, individual sensor calibrations must be performed prior to use, making this less important. Figure 5A presents ACs for two distinct electropolymerized GOx UME sensors manufactured a few months apart (both tested the second day after manufacturing, approaching to plastic Petri dishes) and illustrates overall reproducibility of the electropolymerization manufacturing process. We can compare the ACs since we have the 'zero separation distance' for each curve, and currents have been normalized with respect to their steady-state current values. For the sensor #2 in Figure 5A the current increases upon the tip touching the substrate; this is probably due to a slight compression of the polymer layer which in turn could cause a sudden increase in the concentration of electroactive species at the Pt sensing element. Figures 5B and 5C display ACs for cast electrodes: GOx and LOx cast UME biosensors, respectively. For the case of GOx-based sensors the ACs can be used as means of positioning the tip at a known distance from the substrate when imaging live cells for example (since the solution contains glucose needed for cell viability). In the case of metabolic lactate imaging, there is insufficient lactate in the extracellular solution (e.g., produced by a single cell, since the solution has no added lactate) to allow an AC to be performed, although there might be other applications where the lactate approach curves might find use (e.g., study of LOx kinetics). Upon conducting an extensive review of the literature we were unable to find any published studies featuring ACs generated by enzyme electrodes, therefore Figure 5 presents the first amperometric ACs recorded with enzyme coated UMEs. The ACs for the enzyme-coated UMEs do not obey the classic SECM feedback theory, due to the presence of the polymer layer deposited on the Pt surface. The attempts of fitting the ACs to the simple kinetically limited (and/or mass transfer limited) feedback modes for SECM did not succeed either, pointing to the fact that the processes occurring at the tip are complex, and this opens the door to future studies for unfolding the intricacies of enzyme coupled electrode kinetics for these UME sensors.

We have used the ACs for the GOx UME sensors to position the tip at a certain distance (10 μm) from the glass bottom Petri dish on which fibroblasts were cultured at low density (2000 cells in the entire dish) to permit the imaging of a single fibroblast without interference from neighboring cells. We have used both the visual monitoring of the enzyme UME approaching the surface of the Petri dish with the help of the inverted microscope, and the ACs to find the point where the tip touches the substrate. The problem with only physically lowering the tip

onto the surface of the substrate[37] is that the tip can be damaged in the process. By using the ACs in conjunction with the optical monitoring of the moving tip, we minimize the opportunities for damaging the sensor. Upon establishing physical contact between the tip and the substrate, the tip is retracted the desired distance using the z-axis inchworm of the SECM setup, and consequently the tip-substrate separation distance that we report for the cell imaging is as accurate as the movement of the z-axis inchworm. While it is possible that the polymer layer would slightly adhere to the surface of the dish and the geometry of the enzyme film would be slightly disturbed in the retraction movement, our calibration experiments (Figures 3 and 4) clearly indicate that the analyte sensitivity of the UME biosensor is not altered upon recording ACs and gently touching the surface of the substrate. Upon positioning the UME biosensor at the desired distance above the Petri dish, the tip is rastered across the live cell while monitoring its movement through the optical microscope. Figure 6 shows the results of such an experiment, revealing a glucose uptake profile above a single fibroblast from a background solution containing 5 mM glucose. The current is the lowest on the top of the cell (as expected) and the uptake profile is uniform. The glucose uptake profile above a single fibroblast looks similar to the topography profiles of single fibroblasts. It is possible that the glucose uptake observed here is a combination of both diffusion/distribution profile of glucose around the fibroblast and nutrient uptake by the cell. Consequently, for the study of cell metabolism one should acquire glucose uptake images in conjunction with measuring the cellular production of an analyte, such as lactate.

One of the hallmarks of cancer cells is a lowered extracellular pH which is in part due to increased anaerobic respiration and lactate production by the cell (Figure 1). We have picked for this study an invasive cell line (MCF10CA1a) that forms tumors and metastasis in mice.[50] Figure 7 represents lactate production by a single MCF10CA1a cell, as sensed by a cast LOx 25 μm UME tip. The onset and falloff of current during the scan was observed (via the inverted microscope) to coincide with the period when the UME sensor was physically above the cell. The topography of the MCF10CA1a cells is hemispherical; however, because the lactate is produced by the cell (as opposed to being consumed, as in the case of glucose uptake), an increase in the lactate concentration above the cell is a consequence of cellular activity, and it cannot be mistaken for changes in cellular topography. The overlaid background curve was generated by repeating the scan, at the same tip-substrate separation, in a region of the dish where no cells were present. We chose the control experiment of scanning above the bare surface of the Petri dish in order to prove that unless there is a source for the lactate (i.e., MCF10CA1a cell in our case), no current increase will be observed.

Cancer cells present enhanced aerobic glycolysis[44] and thus oxygen is an important analyte (Figure 1) that has to be accounted for when the metabolic profiling of cancerous cells is sought. We have recorded topographical images of PC12 cells in a medium containing FcTMA, with the potential of the 7 μm Pt UME tip set at E = + 0.6 vs. Ag/AgCl, 3 M KCl; at this potential the FcTMA present in solution gets oxidized at the Pt tip and a topography-type profile is observed, corresponding to the amount of FcTMA available for immediate diffusion to the tip, i.e., corresponding to the distance between the tip and the imaged object (PC12 cell in this case). An example of PC12 topography can be observed in Figure 8A, where the 3D contour plot for the FcTMA oxidation profile around the cell is presented. The shape of the cell appears uniform, as a hemispherical object. Upon obtaining information about the cell surface, we have switched the potential of the same Pt tip to E = − 0.5 vs. Ag/AgCl, 3 M KCl, to ensure the reduction of the oxygen present in solution at the Pt UME, and we have scanned the same area and obtained a respiration profile of the same single PC12 cell as it can be seen in Figure 8B. It is very interesting to observe that the oxygen profile we recorded across the cell does not mirror the topography. Takii et al.[37] reported that the acquired respiration image identically matched the expected topography (profile of the oxygen diffusion hindrance atop the cell, i.e., the oxygen distribution around the cell) and they were not able to show distinctive oxygen

uptake profiles. While we have acquired images (taken at d ≈ 10 μm from the dish surface, not shown) that resemble the previously published cell respiration images as cell topography, when the tip is scanned closer than 10 μm to the surface, it is possible to obtain images that allow differentiation in respiratory activity as a function of spatial location. Since the diffusion of the oxygen is extremely rapid in aqueous solutions, it is important to approach closer to the cell, so that the image obtained (E = − 0.5 vs. Ag/AgCl, 3 M KCl) is not solely the result of the cell topography, but includes oxygen uptake concentration profiles. We have recorded a respiration profile at d ≃ 8 μm from the dish surface, and the respiration image (3D contour plot, Figure 8B) raster shows the lowest respiration activity in the middle of the cell surface, and the highest respiration activity at the edge of the cell, where the cell makes contact with the Petri dish. While this image does certainly have a component that comes from the distribution of the oxygen around the cell, it is obvious that we were able to record the oxygen depletion by the cell. Also, one could argue that the reason we are not observing uniform oxygen diffusion across the cell membrane is due to the higher distribution of mitochondria (where cellular respiratory activity occurs) at the points where the cell makes contact with the Petri dish substrate. Figures 8C and 8D are the corresponding plots for topography (Figure 8A) and respiration (Figure 8B) respectively, and we have inserted crosshairs to better illustrate portions of the 2D profiles. Figure 8C, which uses an external redox mediator and so is independent of physiological activity, shows a clear dependence between the current profile and topography for a roughly spheroid cell. Figure 8D, however, displays a more convoluted oxygen profile that can not be explained solely by topography, and therefore is indicative of physiological activity (i.e., respiration) and/or transport properties of the cell or membrane itself.

CONCLUSIONS

We have manufactured enzyme UMEs for SECM use in the detection of lactate and glucose. We have calibrated these sensors with respect to their analyte and we have shown for the first time that enzyme-based UMEs can be used for positioning the SECM tip via amperometric ACs with respect to the substrate to be scanned. By employing the GOx- and LOx-based UME biosensors, we have obtained glucose uptake and lactate release profiles for single cancer cells as a proof of concept for the application of SECM toward the study of basic metabolic processes that are affected by disease in cancerous cells. We have also shown that respiration studies performed at closer tip-substrate separations (< 10 μm) reveal a non-uniform distribution of oxygen that cannot be explained by the cell topography alone; these oxygen uptake profiles could give a more complete metabolic picture of the single cancer cells. Further experimentation, however, is required to definitively assign this convoluted oxygen uptake distribution to a difference in respiratory activities within the cell itself. The ability to look at single cell lactate production, glucose and oxygen consumption, in addition to previously published acidification rates profiles, will provide for a direct comparison of single cell data to our multi-cell data from MAMP experiments.

Acknowledgments

We thank Evgheni Kozlov/Ales Prokop (fibroblasts and PC12), Julie Maier/Alissa Weaver (MCF10CA1a) and Kristopher Kahlig/Aurelio Galli (PC12) for cell culture and plating. We acknowledge the following funding sources: NIAID U01 AI061223; NCI U54 CA113007; DARPA/ONR contract N66001-01-8064; the Vanderbilt Integrative Cancer Biology Center; and the Vanderbilt Institute for Integrative Biosystems Research and Education.

References

1. Suzuki H. Electroanalysis 2000;12(9):703–715.
2. Lindner E, Buck RP. Anal Chem 2000;72(9):336A–345A.
3. Yao T, Yano T, Nanjyo Y, Nishino H. Anal Sci 2003;19(1):61–65. [PubMed: 12558025]

4. Marzouk SAM, Buck RP, Dunlap LA, Johnson TA, Cascio WE. Anal Biochem 2002;308(1):52–60. [PubMed: 12234463]
5. Garrett, RH.; Grisham, CM. Biochemistry. 2. Saunders College Publishing; Fort Worth: 1999.
6. Chen T, Schmidtke DW, Heller A. Clin Chem Lab Med 2002;40(8):786–789. [PubMed: 12392305]
7. Strike DJ, de Rooij NF, Koudelka-Hep M. Biosens Bioelectron 1995;10(12):61–66.
8. Kueng A, Kranz C, Mizaikoff B. Biosens Bioelectron 2005;21(2):346–353. [PubMed: 16023962]
9. Ito N, Matsumoto T, Fujiwara H, Matsumoto Y, Kayashima S, Arai T, Kikuchi M, Karube I. Anal Chim Acta 1995;312(3):323–328.
10. Horrocks BR, Schmidtke D, Heller A, Bard AJ. Anal Chem 1993;65(24):3605–3614. [PubMed: 8311247]
11. Devadoss A, Burgess JD. J Am Chem Soc 2004;126(33):10214–10215. [PubMed: 15315412]
12. Jiang D, Devadoss A, Palencsar MS, Fang D, White NM, Kelley TJ, Smith JD, Burgess JD. J Am Chem Soc 2007;129(37):11352–11353. [PubMed: 17718573]
13. Eklund SE, Cliffel DE, Kozlov E, Prokop A, Wikswo J, Baudenbacher F. Anal Chim Acta 2003;496 (1–2):93–101.
14. Eklund, SE.; Kozlov, E.; Taylor, DE.; Baudenbacher, F.; Cliffel, DE. Methods in Molecular Biology. In: Rosenthal, SJ.; Wright, DW., editors. NanoBiotechnology Protocols. Vol. 303. Humana Press, Inc; Totowa: 2005. p. 209-223.
15. Eklund SE, Snider RM, Wikswo J, Baudenbacher F, Prokop A, Cliffel DE. J Electroanal Chem 2006;587(2):333–339.
16. Eklund SE, Taylor D, Kozlov E, Prokop A, Cliffel DE. Anal Chem 2004;76(3):519–527. [PubMed: 14750842]
17. Anderson ARA. Math Med Biol 2005;22(2):163–186. [PubMed: 15781426]
18. Anderson ARA, Weaver AM, Cummings PT, Quaranta V. Cell 2006;127(5):905–915. [PubMed: 17129778]
19. Kueng A, Kranz C, Lugstein A, Bertagnolli E, Mizaikoff B. Angew Chem, Int Ed Engl 2005;44(22): 3419–3422. [PubMed: 15861452]
20. Bard AJ, Fan FRF, Kwak J, Lev O. Anal Chem 1989;61(2):132–138.
21. Bard, AJ.; Fan, FRF.; Mirkin, MV. Electroanalytical Chemistry. Vol. 18. Marcel Dekker, Inc; New York: 1994. p. 243-373.
22. Bard AJ, Fan FRF, Pierce DT, Unwin PR, Wipf DO, Zhou F. Science 1991;254(5028):68–74. [PubMed: 17739954]
23. Bard, AJ.; Mirkin, MV. Scanning Electrochemical Microscopy. Marcel Dekker, Inc; New York: 2001.
24. Shiku, H.; Ohya, H.; Matsue, T. Bioelectrochemistry. Vol. 9. WILEY-VCH; Weinheim, Germany: 2002. Encyclopedia of Electrochemistry; p. 257-275.
25. Bard AJ, Li X, Zhan W. Biosens Bioelectron 2006;22(4):461–472. [PubMed: 16797958]
26. Cai C, Liu B, Mirkin MV, Frank HA, Rusling JF. Anal Chem 2002;74:114–119. [PubMed: 11795778]
27. Feng W, Rotenberg SA, Mirkin MV. Anal Chem 2003;75:4148–4154. [PubMed: 14632128]
28. Hengstenberg A, Blochl A, Dietzel ID, Schuhmann W. Angew Chem, Int Ed Engl 2001;40(5):905–908. [PubMed: 11241642]
29. Isik S, Schuhmann W. Angew Chem, Int Ed Engl 2006;45(44):7451–7454. [PubMed: 17039552]
30. Kurulugama RT, Wipf DO, Takacs SA, Pongmayteegul S, Garris PA, Baur JE. Anal Chem 2005;77 (4):1111–1117. [PubMed: 15858993]
31. Liebetrau JM, Miller HM, Baur JE, Takacs SA, Anupunpisit V, Garris PA, Wipf DO. Anal Chem 2003;75:563–571. [PubMed: 12585485]
32. Liu B, Cheng W, Rotenberg SA, Mirkin MV. J Electroanal Chem 2001;500:590–597.
33. Liu B, Rotenberg SA, Mirkin MV. Proc Natl Acad Sci USA 2000;97(18):9855–9860. [PubMed: 10963658]
34. Liu B, Rotenberg SA, Mirkin MV. Anal Chem 2002;74:6340–6348. [PubMed: 12510757]
35. Mauzeroll J, Bard AJ, Owhadian O, Monks TJ. Proc Natl Acad Sci USA 2004;101(51):17582–17587. [PubMed: 15601769]
36. Nishizawa M, Takoh K, Matsue T. Langmuir 2002;18(9):3645–3649.

37. Takii Y, Takoh K, Nishizawa M, Matsue T. Electrochim Acta 2003;48:3381–3385.
38. Yasukawa T, Kaya T, Matsue T. Electroanalysis 2000;12(9):653–659.
39. Wipf DO, Bard AJ. Anal Chem 1992;64(13):1362–1367.
40. Ludwig M, Kranz C, Schuhmann W, Gaub HE. Rev Sci Instrum 1995;66(4):2857–2860.
41. Hengstenberg A, Kranz C, Schuhmann W. Chemistry--A European Journal 2000;6(9):1547–1554.
42. Macpherson JV, Unwin PR. Anal Chem 2001;73(3):550–557. [PubMed: 11217761]
43. Semenza, GL.; Artemov, D.; Bedi, A.; Bhujwalla, Z.; Chiles, K.; Feldser, D.; Laughner, E.; Ravi, R.; Simons, J.; Taghavi, P.; Zhong, H. The Tumour Microenvironment: Causes and Consequences of Hypoxia and Acidity, Novartis Foundation Symposium; 2001. p. 251-260.discussion 260–264
44. Warburg, O. The metabolism of tumors. Constable; London: 1930.
45. Griffiths, JR.; McIntyre, DJO.; Howe, FA.; Stubbs, M. The Tumour Microenvironment: Causes and Consequences of Hypoxia and Acidity, Novartis Foundation Symposium; 2001. p. 46-62.discussion 62–67
46. Bhujwalla, ZM.; Artemov, D.; Aboagye, E.; Ackerstaff, E.; Gillies, RJ.; Natarajan, K.; Solaiyappan, M. The Tumour Microenvironment: Causes and Consequences of Hypoxia and Acidity, Novartis Foundation Symposium; 2001. p. 23-38.discussion 38–45
47. Walenta S, Salameh A, Lyng H, Evensen JF, Mitze M, Rofstad EK, Mueller-Klieser W. Am J Pathology 1997;150(2):409–415.
48. Forouzan F, Bard AJ, Mirkin MV. Isr J Chem 1997;37:155–163.
49. Zhang Z, Liu H, Deng J. Anal Chem 1996;68(9):1632–1638.
50. Santner SJ, Dawson PJ, Tait L, Soule HD, Eliason J, Mohamed AN, Wolman SR, Heppner GH, Miller FR. Breast Cancer Res Treatment 2001;65(2):101–110.
51. Wilburn JP, Wright DW, Cliffel DE. Analyst 2006;131(2):311–316. [PubMed: 16440098]
52. Bard, AJ.; Faulkner, LR. Electrochemical Methods: Fundamentals and Applications. 2. John Wiley & Sons, Inc; New York: 2001.

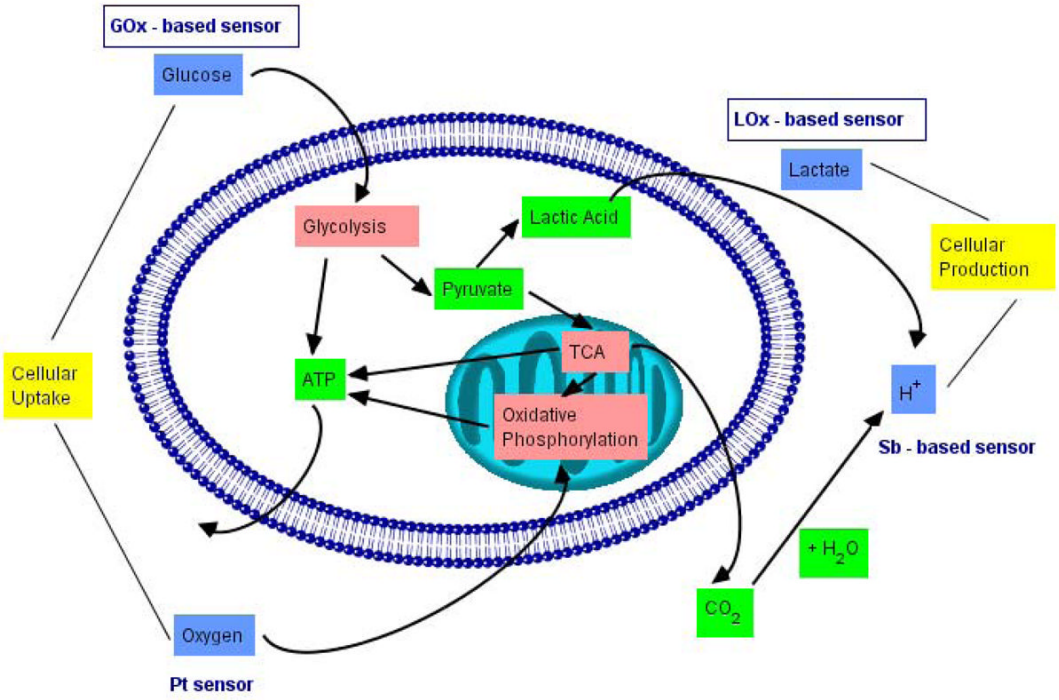

Figure 1.

Cancer cell metabolic pathways suitable for electrochemical probing by SECM. Cancer cells have an altered metabolism compared to normal cells, with glycolysis being one of the affected pathways. TCA = tricarboxylic acid cycle.

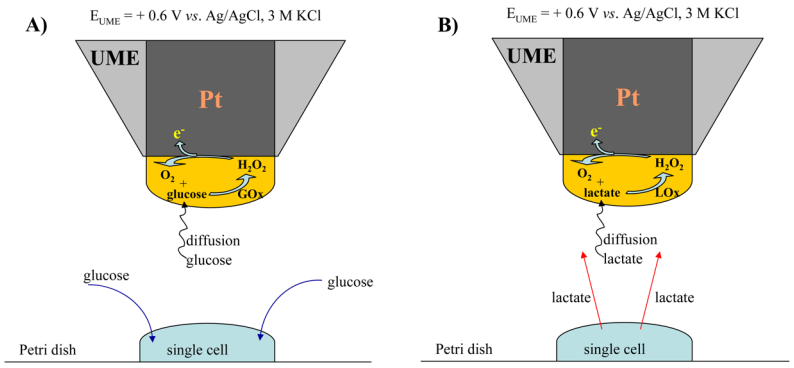

Figure 2.

Enzyme-based UME biosensor. Enzyme layer (GOx (A) or LOx (B)) is deposited onto 25 μm Pt UME by either electropolymerization or casting. The tip is rastered across the cell adhered to a Petri dish: A) in the case of GOx it senses extracellular glucose depletion due to cellular uptake; B) in the case of LOx it senses lactate production by the cell. The enzyme film breaks down the analyte, and the resulting H_2O_2 is oxidized at the underlying Pt UME. The arrows entering the cell symbolize glucose uptake (A), while the arrows exiting the single cell denote lactate production (B).

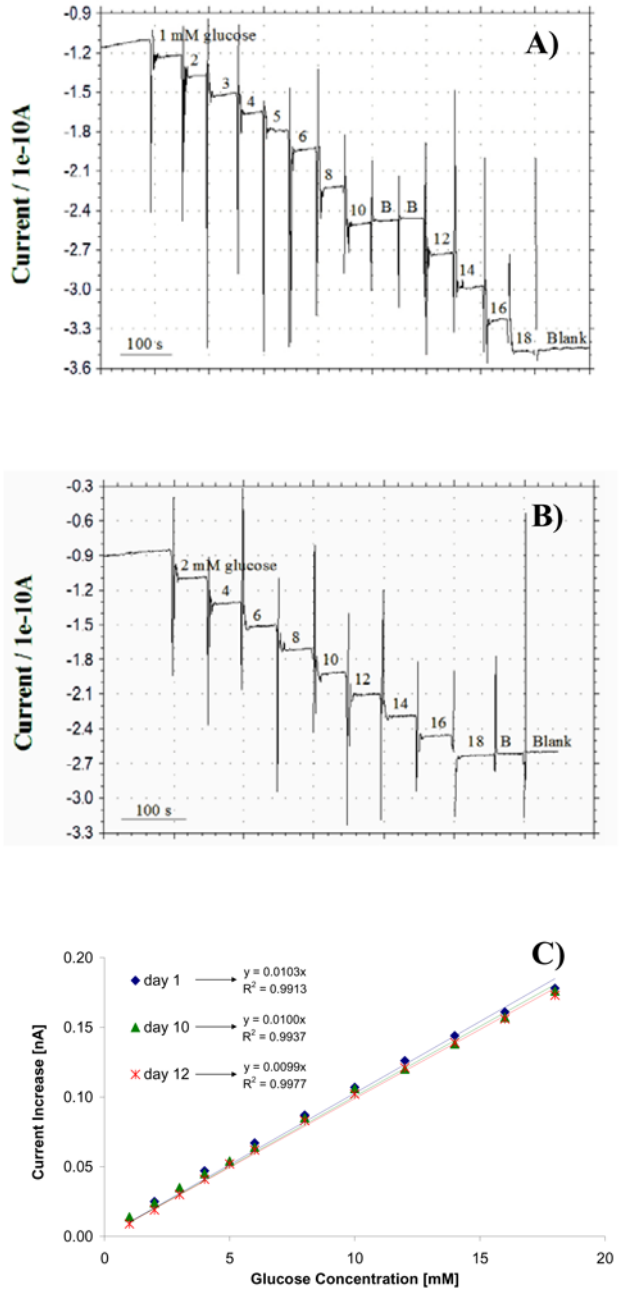

Figure 3.

Amperometric calibrations of electropolymerized GOx 25 μm UME biosensors, E = + 0.6 *vs*. Ag/AgCl, 3 M KCl; additions up to 18 mM glucose in 50 mM phosphate buffer, pH 7: A) GOx UME sensors exhibit sensitivity to glucose prior to SECM experiments; B) the sensors preserve the sensitivity to their analyte after being employed in extensive SECM experiments; C) the electropolymerized GOx biosensors are stable in time when stored in 50 mM phosphate buffer, pH 7 at 4 °C for periods of at least two weeks; same sensor shows almost identical sensitivity after 1, 10 and 12 days from electropolymerization date. The data presented in this figure is for three distinct electropolymerized GOx sensors (one sensor for the data in (A), one sensor for the data in (B), and another sensor for the data in (C)).

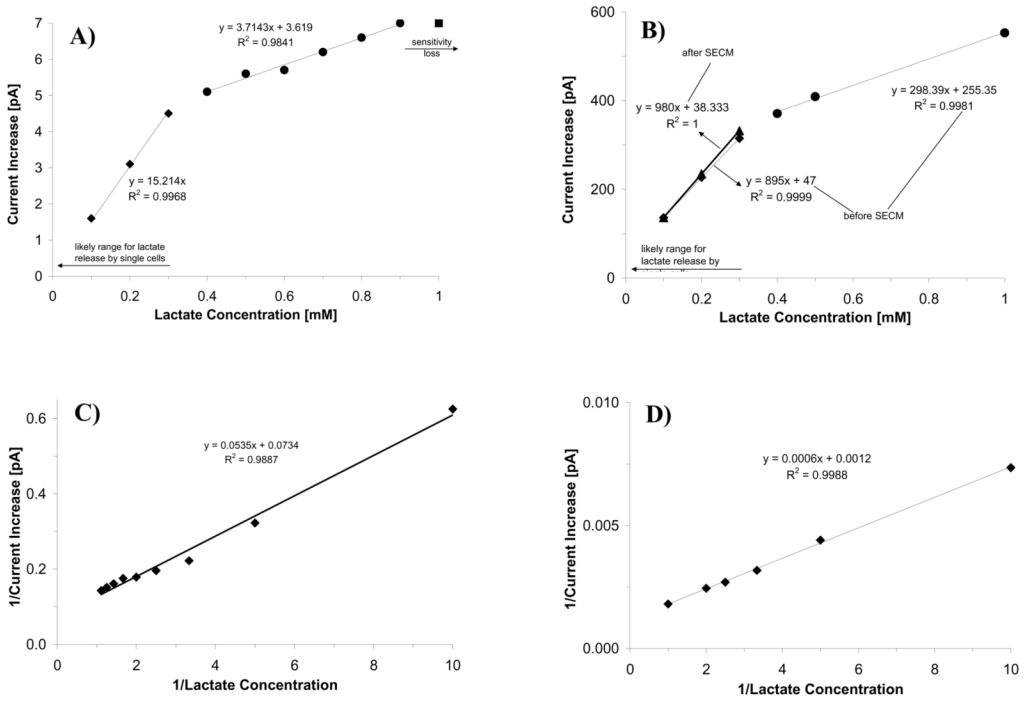

Figure 4.

Amperometric calibrations of A) electropolymerized and B) cast LOx 25 μm UME biosensors, E = + 0.6 *vs*. Ag/AgCl, 3 M KCl; additions up to 1 mM lactate in 50 mM phosphate buffer, pH 7. The sensors were calibrated for concentrations of up to 1 mM lactate, and display two distinct linear regions: below 0.3 mM and above 0.4 mM, with the expected cellular lactate release range below 0.3 mM. The sensors retain lactate sensitivity upon being used in SECM experiments. Double reciprocal plot representations of these amperometric calibrations: C) the electropolymerized LOx sensor for which the corresponding data is shown in A); and D) cast LOx sensor for which the corresponding data is shown in B) – before use in SECM.

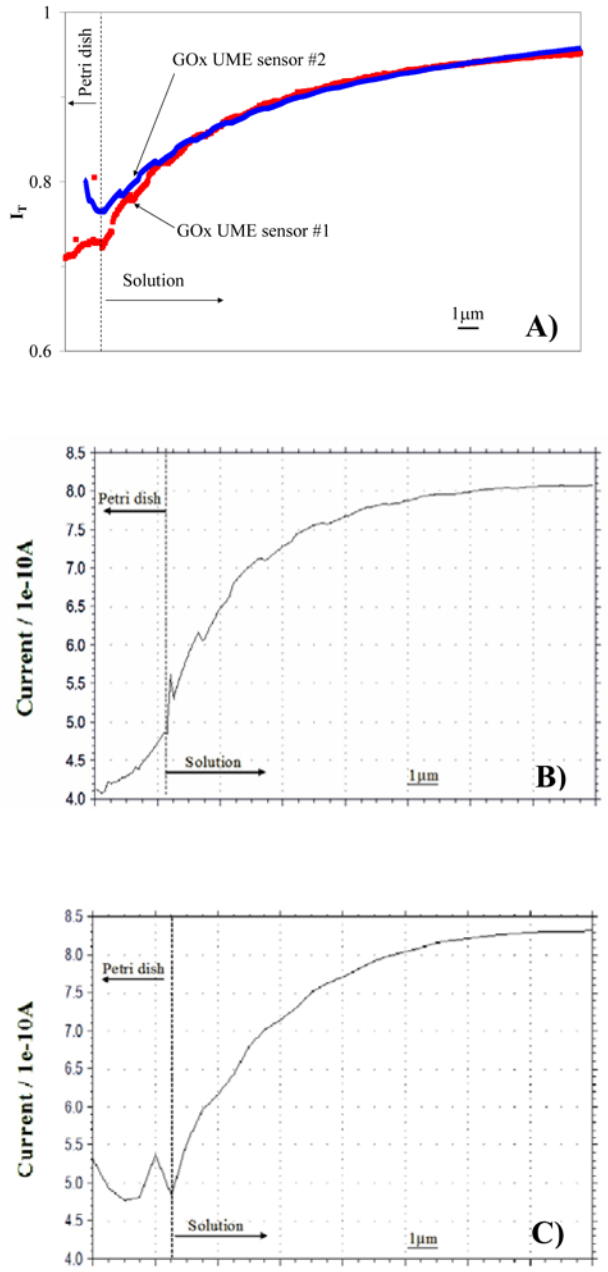

Figure 5.

Approach curves for 25 μm UME enzyme-based biosensors; E = + 0.6 *vs*. Ag/AgCl, 3 M KCl; in 50 mM phosphate buffer, pH 7: A) GOx electropolymerized sensors #1 (approach speed 1.5 μm/s) and #2 (approach speed 3 μm/s) yielded similar curves in 5 mM glucose, indicating reproducibility; B) GOx cast sensor (5 mM glucose, approach speed 3 μm/s); C) LOx cast (0.5 mM lactate, approach speed 15 μm/s). In all plots the vertical dashed line represents the point where the UME tip touches the Petri dish, coming from the right side (solution side).

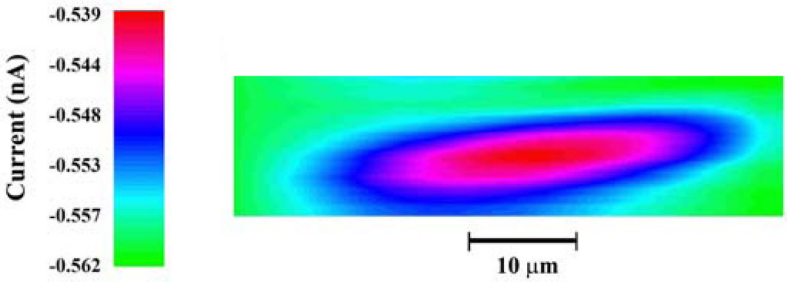

Figure 6.

Glucose uptake profile for a single fibroblast. E = + 0.6 *vs*. Ag/AgCl, 3 M KCl; 5 mM glucose in HBSS, pH 7.4; scanning speed 15 μm/s; tip: GOx cast film on 25 μm UME biosensor; d = 10 μm from Petri dish; data have been corrected for background tilt in Origin Pro 7.5. The GOx cast 25 μm UME tip was positioned at 10 μm from the Petri dish by using approach curves.

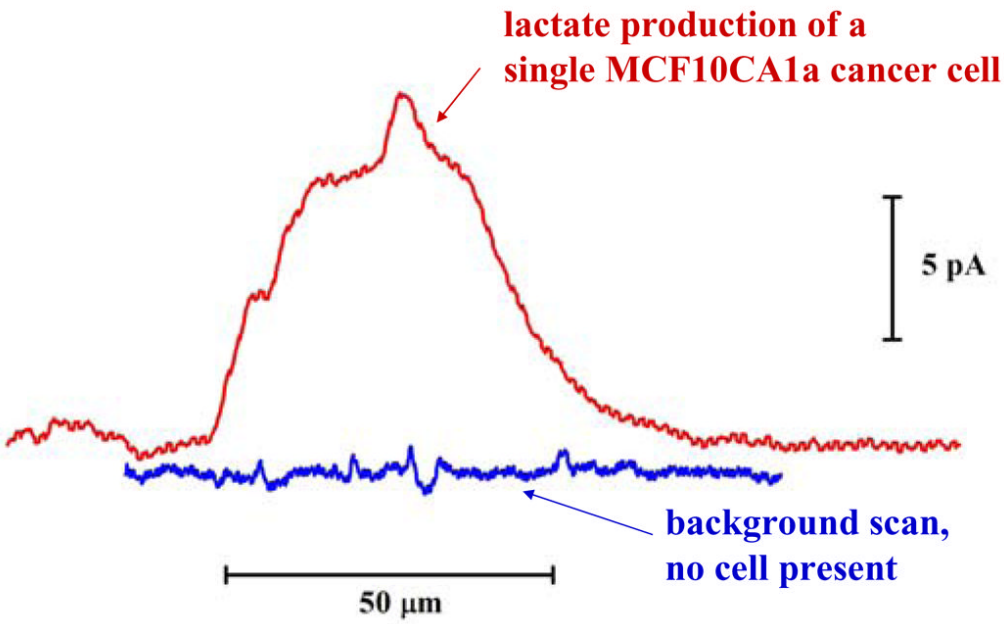

Figure 7.

Lactate production from a single cancer cell MCF10CA1a. E = + 0.6 *vs.* Ag/AgCl, 3 M KCl; no lactate added in RPMI media, pH 7.4; scan speed 3 µm/s; tip: LOx cast film on 25 µm UME biosensor; red line: lactate production current associated with a single MCF10CA1a cancer cell; blue line: in the same Petri dish, same electrode, scan across surface when no cancer cells are present in the path of the electrode; data have been corrected for background tilt in Origin Pro 7.5.

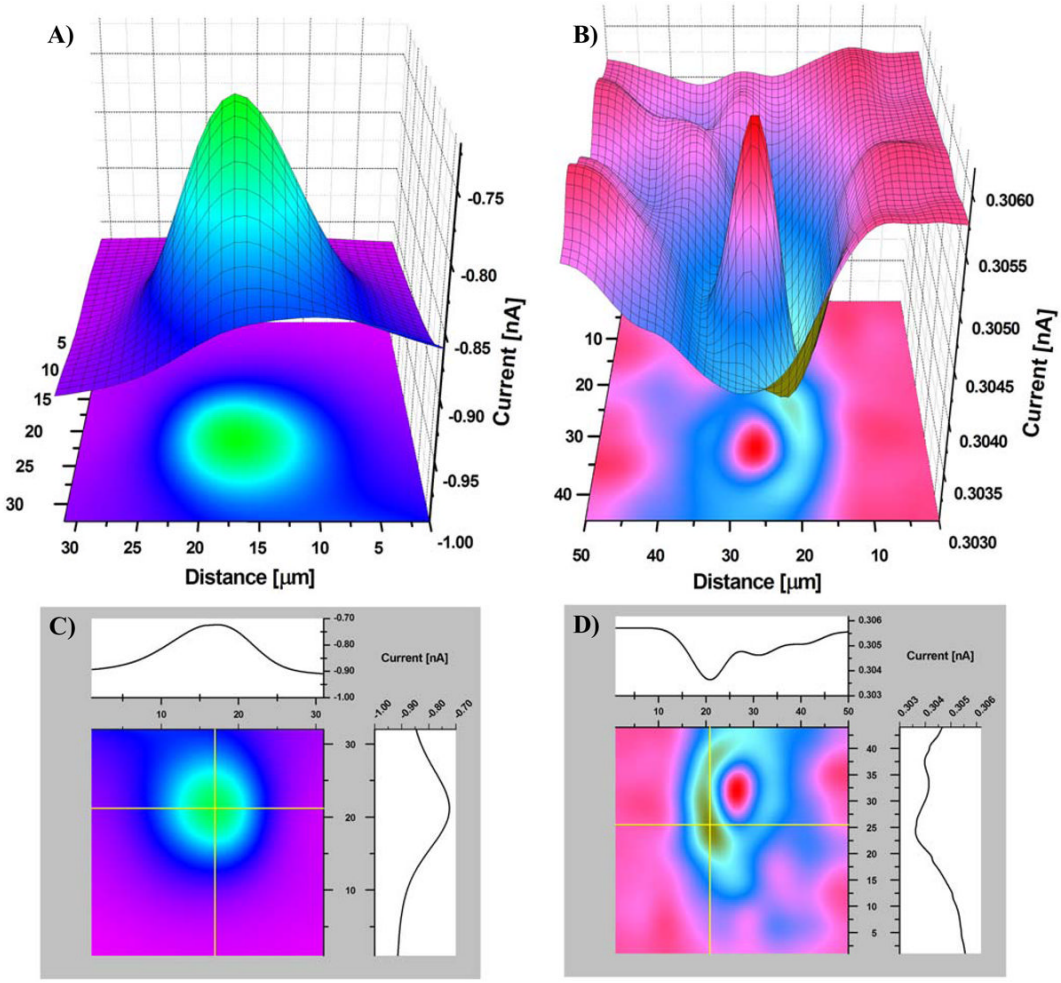

Figure 8.

Topography (A and C) and oxygen uptake profile (B and D) of a single PC12 cell. E = + 0.6 vs. Ag/AgCl, 3 M KCl for topography and E = − 0.5 *vs*. Ag/AgCl, 3 M KCl for respiration; 1 mM FcTMA in Ringer's solution pH 7.4; tip: Pt 7 μm UME and scanning speed 30 μm/s for both images; data have been corrected for background tilt in Origin Pro 7.5. The tip was positioned by ACs to the insulating Petri dish surface: d ≃ 10 μm from Petri dish for topography and d ≃ 8 μm from Petri dish for respiration. A and B display the 3D contour plots for topography and respiration respectively. C and D are the same images from A and B with 'crosshairs' for easier comparison of the topography and respiration profiles: horizontal crosshair corresponds to the scan presented above the image; vertical crosshair corresponds to the scan presented on the right side of the image. All distances are in μm.